Multiscale constraints on scalar-field couplings to matter: The geodetic and frame-dragging effects

David Benisty,[1,2,*] Philippe Brax,[3,4,†] and Anne-Christine Davis[1,2,‡]

[1]*DAMTP, Centre for Mathematical Sciences, University of Cambridge, Wilberforce Road, Cambridge CB3 0WA, United Kingdom*
[2]*Kavli Institute of Cosmology (KICC), University of Cambridge, Madingley Road, Cambridge, CB3 0HA, United Kingdom*
[3]*Institut de Physique Theorique, Universite Paris-Saclay, CEA, CNRS, F-91191 Gif-sur-Yvette Cedex, France*
[4]*CERN, Theoretical Physics Department, Geneva, Switzerland*

(Received 9 June 2023; accepted 6 September 2023; published 27 September 2023)

The impact of light scalars coupled conformally and disformally to matter on the geodetic and frame-dragging precessions is calculated. For larger frequencies the disformal interaction becomes increasingly relevant. We use several satellite experiments and pulsar time of arrival measurements to derive bounds on the couplings, combining the Gravity Probe B, LARES, LAGEOS and GRACE results with pulsar timings. Forecasts for future constraints on the conformal and the disformal couplings based on the GINGER experiment, i.e. a future measurement of the Sagnac effect on Earth, the motion of *S* stars around the Galactic Center and future pulsar timing observations are presented.

DOI: 10.1103/PhysRevD.108.063031

I. INTRODUCTION

Einstein's theory of general relativity (GR) has been probed using gravitational tests in the solar system and within galactic environments—most recently by the gravitational wave detection. Despite its resounding success in describing the present day Universe, GR's connection to both early and late time phenomena is problematic. Examples can be found in the early Universe with the unexplained nature of the big bang singularity or the initial conditions that would give rise to the standard model of big bang cosmology. Another area where GR does not give a definite answer is the nature of the accelerated expansion of the Universe [1,2]. The famous and mysterious component of the Universe called dark energy does not have a consistent microscopic model within quantum field theory and GR [3]. Both of these reasons have motivated the study of extensions of GR in different astrophysical systems [4,5].

The class of theories we are broadly interested in here can obey current observational constraints and mimic GR when they exhibit screening effects whereby the modifications to GR are hidden at small scales. Observed large scales are mostly unaffected by the modification of gravity apart from some interesting and small effects on the growth of structure. More specifically, in this paper we focus on theories where the conformal coupling to matter depends on the environment, i.e. the distribution of matter around the considered objects, e.g. satellites in the Earth's atmosphere or pulsars in the Milky Way.[1] The most general coupling of a scalar field to matter is obtained via the conformal and disformal terms as appearing in the Jordan frame metric as shown by Bekenstein in [7]. Such theories give rise to fifth forces generically, which are subject to strict limits by solar system tests of GR [8]. Consequently, the effect of fifth forces need to be screened in the solar system, giving rise to screened modified gravity models. Such models can be screened via various mechanisms [9–14]. All rely in different ways on the environment and are such that the fifth force is screened in the solar system, i.e. the theory evades all solar system tests, and can give rise to modifications to GR on cosmological scales. Similarly the disformal coupling to matter gives rise to modifications to GR which can be constrained from the solar system to collider physics [15,16]. This results in constraints on the

*db888@cam.ac.uk
†philippe.brax@ipht.fr
‡ad107@cam.ac.uk

[1]For a description of these models and a comparison with scalarization, see [6].

disformal coupling to matter [17–25] and forecasts for future satellite experiments [26,27].

We analyze the effect of both the conformal and disformal couplings on the geodetic and frame-dragging (FD) precessions. Current astrophysical observations are used to constrain the coupling strengths in the conformal and disformal cases. In practice, we consider scalar-tensor theories of gravity and their effect on the precession frequency of rotating gravitating objects [28]. The Jordan metric $g^J_{\mu\nu}$ is related to the Einstein metric thanks to the metric transformation [7,19,23,29]:

$$g^{(J)}_{\mu\nu} = \left(1 + 2\beta\frac{\phi}{m_{\rm Pl}}\right) g^{(E)}_{\mu\nu} + \frac{2}{m^2_{\rm Pl}\Lambda^2}\partial_\mu\phi\partial_\nu\phi, \qquad (1)$$

where $g^{(J)}_{\mu\nu}$ is the metric in Jordan frame and $g^{(E)}_{\mu\nu}$ is the metric in the Einstein frame. β is conformal coupling strength with matter, which will depend on the environment, and Λ is the disformal coupling strength with matter. We have denoted by $m_{\rm Pl}$ the Planck mass. Notice that β is dimensionless and Λ has dimension of mass. Recently, light scalar fields have also been suggested as possible candidates for dark matter [30]. The coupling of such dark matter fields to matter is also crucial for their dynamics and their eventual detection [31–33].

These theories can be tested using gravitational methods as shown by earlier studies which focused on two bodies in an orbital motion [34–41], a well studied example in GR, from which similar properties can be inferred for light scalars with conformal and disformal couplings [6,15,42–48].

We will focus on tests of the geodetic and the FD effects. The geodetic effect [or de Sitter (dS)] follows from the curvature of spacetime predicted by general relativity, and the way it acts on a vector carried along with an orbiting body [49,50]. The FD, or Lense-Thirring, effect is one of the main predictions of Einstein's theory of gravitation in the limit of weak field and slow motion, i.e. it represents a tiny relativistic precession of the orbital plane of a satellite produced by the angular momentum of the primary object [51–57]. The difference between the geodetic and FD effects is that the de Sitter one is due simply to the presence of a central mass, whereas FD precession is due to the rotation of the central mass. The total precession is calculated by combining the de Sitter precession with the FD precession. The precessions read in GR

$$\Omega_{dS} = \frac{3Gn_b}{2ac^2(1-e^2)}\frac{m_2(4m_1+3m_2)}{(m_1+m_2)^{4/3}}, \qquad (2a)$$

$$\Omega_{\rm FD} = \frac{3GS}{2ac^2(1-e^2)^{3/2}}, \qquad (2b)$$

where G is the Newtonian constant, $n_b = 2\pi/P_b$ is the orbital frequency, a is the semimajor axis, c is the speed of light, e is the eccentricity, S is the spin of the central body and $m_{1,2}$ are the masses of the bodies. The directions of the vectors are

$$\vec{\Omega}_{dS} = \Omega_{dS}\vec{k}, \qquad \vec{\Omega}_{\rm FD} = \Omega_{\rm FD}(\vec{s}' - 3(\vec{k}\cdot\vec{s}')\vec{k}), \qquad (3)$$

where $\vec{k} = \vec{J}/J$ is the unit vector along the orbital angular momentum, $\vec{J}$ is the orbital angular momentum and $\vec{s}$ is the spin vector of the companion body.

Reference [15] has extended the leading order calculations in GR to include both conformal and disformal couplings to matter in scalar-tensor theories applied to the two-body problem in the post-Newtonian expansion. This enables one to test these theories in new regimes, such as the Galactic Center where stars and the supermassive black hole orbit around each other [58]. Reference [6] derives the corresponding post-Keplerian parameters and the influence of the conformal and disformal couplings. The higher derivative nature of the disformal interaction is parametrized using the dimensionless quantity ϵ_Λ which relates the disformal coupling interaction to the frequency

$$\epsilon_\Lambda = \frac{(\beta\cdot n_b/\Lambda)^2}{(1-e^2)^3}, \qquad (4)$$

where $n_b = 2\pi/P_b$ is the frequency of the motion and P_b is the period of the motion. ϵ_Λ parametrizes the contributions of the disformal interaction to the post-Keplerian parameters (PKP). As we will see, this parameter also appears naturally in the geodetic and in the FD terms. Figure 1 compares the experiment that we discuss in this paper and in particular the relative error of the precession rate vs the orbital period. For larger n_b with lower errors the bound on the disformal coupling is expected to be the strongest.

Notice that the bounds derived here from satellite experiments are not as strong as the ones obtained in

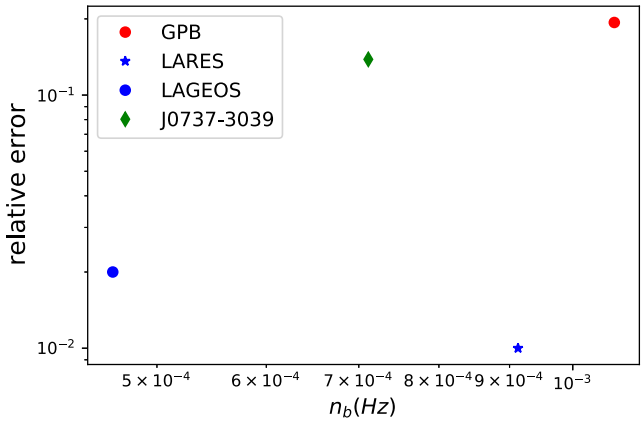

FIG. 1. Comparison of the geodetic and the frame dragging measurements from different datasets that are discussed in this paper: We give the accuracy of the experiment vs the orbital frequency.

particle physics [16] or even with pulsar timings [6]. The particle physics and pulsar timing results involve energies and environments which differ from the ones in the solar system tests. As such the results presented here complement the known bounds on the conformal and disformal couplings and are environment specific.[2]

The structure of this paper is as follows: Section II calculates the geodesic and the frame-dragging effects for scalar tensor theories with conformal and disformal interactions. Section III describes the constraints on the interactions from current and future satellites experiments. Section IV discusses the GINGER experiment in details. Section V considers the binary pulsars and their current and future constraints. Section VI discusses the possible detection of effects in the Galactic Center, and finally Sec. VII summarizes current and future results.

II. LIGHT SCALARS INTERACTING WITH MATTER

A. The interactions

The dynamics of gravity interacting with a massless scalar field are described by

$$S=\int d^4x\sqrt{-g}\left(m_{\rm Pl}^2\frac{R}{2}-\frac{1}{2}g^{\mu\nu}\phi_{,\mu}\phi_{,\nu}\right)+S_m(\psi_i,g^J_{\mu\nu}), \quad (5)$$

where matter fields are denoted by ψ_i and their action by S_m. In the following we will take the matter action to be the one of pointlike particles and the scalar potential to be vanishing. In particular, we take the mass of the scalar field to be vanishing. In practice, we assume that the Compton wavelength $1/m$ of the scalar field, where m is the scalar mass, is much larger than the scales we are considering. Typically, scalar effects are Yukawa suppressed by an exponential term e^{-mr}, where r is the distance to a gravitational source and therefore no scalar effects are expected if $r\lesssim m^{-1}$. We focus on the regime where the dynamics of the scalar are not Yukawa suppressed and thus will simply take the mass to be vanishing. This will provide an appropriate description of the dynamics of macroscopic objects like neutron stars as long as finite size effects can be neglected. This setting can also apply to screened models where the scalar field between massive objects is assumed to be very light and the coupling to matter reduced by the appropriate screening mechanism in order to pass solar system tests of gravitation. In particular, we consider that β depends on the environment, i.e. it could be different around a pulsar and in the solar system, see [6] for a more thorough discussion, hence the bounds that we will deduce are specific to the given environment of each of the considered binary systems. Here we take β to be universal, i.e. it does not depend on the nature of the objects but only of their environment. The case of nonuniversal couplings proportional to the inverse compactness of the objects is highly relevant to the screened phase of modified gravity models [6]. One of the main effects of taking nonuniversal couplings for different objects would be the dipolar power loss for the binary system which would not vanish and would affect the time evolution of binary pulsars. This would of course affect the parameter space of the models. This is left for future work.

In the following, we will be interested in precession effects for bound orbits, e.g. binary systems. The metric and the scalar field will be treated in perturbation theory where several parameters govern the corresponding expansions. First of all, we will expand in the conformal coupling β^2 which is considered to be small. We will also consider the post-Newtonian expansion (PN) in the small velocities $v^2\simeq GM/r$ for bound orbits where v is a typical speed, M a typical mass and r is the size of the orbit. The disformal interactions will also be taken perturbatively in a ladder expansion [15]. This expansion is valid when the ladder parameter

$$\epsilon_L=\left(\frac{v}{c}\right)^2\frac{GM}{r^3\Lambda^2} \quad (6)$$

is small. When this is not the case, a summation of the ladder contributions must be performed as in [59]. Here we will consider situations where $v/c\ll 1$ and the Newtonian potentials are $GM/r\ll 1$ on the orbits of the binary systems. Moreover, Λ plays the role of a ultraviolet cutoff of the theory above which higher order derivative corrections to the disformal coupling are expected. As a result we focus on the low energy regime $r\Lambda\gg 1$ implying that the ladder parameter is safely lower than unity. Finally, we only consider spin effects at leading order.

B. Spin precession of coupled scalars

General relativity predicts the rotational drag of inertial frames in the vicinity of a rotating object. The precession caused by this rotational drag in the motion of a rotating object is the FD effect. Gyroscopes are test objects which are sensitive to this effect. A gyroscope is nothing but a rotating test particle with spin and we can derive the precession of the spin vector using the Mathisson-Papapetrou-Dixon equations as done in [28,60]. The evolution equation for the dynamics of a spinning test body is given by

$$\dot{p}_\mu=-\frac{1}{2}R^J_{\mu\nu\rho\sigma}u^\nu S^{\rho\sigma} \quad (7)$$

and

[2]This is particularly relevant for models where the couplings are environment dependent such as symmetrons [11], for instance.

$$\dot{S}^{\mu\nu} = 2p^{[\mu}u^{\nu]}, \tag{8}$$

where p^μ is the 4-momentum, u^μ is the 4-velocity, $S^{\mu\nu}$ is the spin angular momentum, and $R_J^{\mu\nu\rho\sigma}$ is the Riemann tensor of the Jordan frame metric, i.e. the metric felt by the spinning particle. The time derivative is taken along the particle world line as $\frac{d}{d\tau} = u^\mu \nabla_\mu$, where τ is the proper time.

We can eliminate the gauge degrees of freedom by imposing the spin supplementary condition (SSC) [28,61,62], $S^{\mu\nu}p_\nu \approx 0$. At leading order in the spin we can write the first step of an iteration scheme as follows [63]:

$$\dot{u}_\mu = 0 + \cdots \tag{9}$$

and

$$\dot{S}_{\mu\nu} = 0 + \cdots, \tag{10}$$

where the neglected terms are of higher order in the spin. This implies that the spin is parallel transported. This also simplifies the SSC to

$$S^{\mu\nu}u_\nu \approx 0 \tag{11}$$

which is preserved along the particle world line $\frac{d}{d\tau}(S^{\mu\nu}u_\nu) = 0$ guaranteeing that the correct number of degrees of freedom is preserved. Indeed, the spin tensor can be projected onto the Pauli-Lubanski vector as

$$S_\mu = -\frac{1}{2}\epsilon_{\mu\nu\rho\sigma}u^\nu S^{\rho\sigma}. \tag{12}$$

This encodes the three independent degrees of freedom which remain after imposing the SSC. We will focus on the components of the spin vector in a comoving tetrad frame. For the weakly rotating bodies that are considered here we have

$$g^J_{\mu\nu} = \eta_{\mu\nu} + h^J_{\mu\nu} \tag{13}$$

and the tetrad vectors

$$e^0_{\hat{i}} = \left(1 + \frac{1}{2}v^2 + h^J_{00}\right)v_i + \frac{1}{2}h^J_{ij}v^j + h_{0i,J} + \mathcal{O}(v^5) \tag{14}$$

$$e^i_{\hat{j}} = \delta^i_j + \frac{1}{2}(v^i v_j - h^i_{j,J}) + \mathcal{O}(v^4), \tag{15}$$

where $e^\mu_{\hat{0}} = u^\mu$, $v^\mu = u^\mu/u_0$ and the hatted indices apply to the local frame. This allows one to project onto the comoving frame. In this case, the spin evolution equation in the comoving frame (10) becomes

$$\frac{d}{d\tau}S_{\hat{i}} = (\Omega \times S)_{\hat{i}} \tag{16}$$

and the resulting precession [28,60]

$$\Omega^{\hat{i}}_A = \frac{1}{4}\epsilon^{ijk}\left(v^j_A \partial_k h^J_{00} - 2v^\mu_A \partial_j h^J_{k\mu}\right) \tag{17}$$

as a function of the velocity of the spinning particle A. This can be separated, at leading order in the velocity, as

$$\vec{\Omega}^G_A = \frac{1}{4}\vec{v}_A \times \vec{\nabla} h^J_{00} \tag{18}$$

which would correspond to the geodetic precession in GR. Similarly, one can introduce the analog of the FD as it would appear in GR:

$$\vec{\Omega}^{\rm FD}_A = -\frac{1}{2}v^0_A(\vec{\nabla} \times \vec{A}_J), \tag{19}$$

where we have introduced the vector $A^i_J = h^J_{0i}$. When the scalar field couples to matter, the metric is influenced by the conformal and disformal terms. Decomposing the metric and the scalar field around a flat background

$$g_{\mu\nu} = \eta_{\mu\nu} + h_{\mu\nu}, \qquad \phi = 0 + \varphi, \tag{20}$$

the Jordan metric becomes

$$g^J_{\mu\nu} = \eta_{\mu\nu} + h^J_{\mu\nu}, \tag{21}$$

where we have introduced

$$h^J_{\mu\nu} = h_{\mu\nu} + 2\beta\frac{\varphi}{m_{\rm Pl}}\eta_{\mu\nu} + \frac{2}{m^2_{\rm Pl}\Lambda^2}\varphi_{,\mu}\varphi_{,\nu} + \cdots. \tag{22}$$

At leading order we have for an N-body system

$$\varphi = -\frac{\beta}{4\pi m_{\rm Pl}}\sum_A \frac{m_A}{|\vec{r} - \vec{r}_A|}, \tag{23}$$

where the bodies are located at $\vec{r}_A$. For a two-body system, we find that the total precession of the first body induced by the scalar field, excluding the spin effects that we will discuss below, is proportional to the angular momentum of the body,

$$\Delta\vec{\Omega}^{dS} \equiv \vec{\Omega}^G + \vec{\Omega}^{\rm FD} = \beta^2 G m_2^2\left(-\frac{r^3}{m_1 + m_2} + \frac{4G}{\Lambda^2 r^6}\right)\vec{\ell}, \tag{24}$$

where r is the distance between the two bodies and $\vec{\ell} = \vec{r} \times \vec{v}$. This is a spin-orbit effect. Notice that there are two contributions including one involving the disformal coupling. We retrieve the result of [28] where

$$\bar{c} = 2\beta, \qquad \frac{\bar{d}}{M^4} = \frac{2}{m_{\rm Pl}^2\Lambda^2} = \frac{4\pi G}{\Lambda^2}. \tag{25}$$

This de Sitter effect is complemented by the frame-dragging effect whose origin follows from the way the spin sources the scalar field in the Klein-Gordon equation.

The FD effect due to the spins of the bodies affects the precession vector. This contribution is mediated by the scalar field via h^J_{00} and its dependence on the spin of the objects which sources the scalar field [28] via the disformal interaction. In the case of a satellite revolving around the Earth, the extra precession is given by

$$\Delta\vec{\Omega}^{\rm FD} = -\frac{4\beta^2 G^2 m_s}{r^6\Lambda^2}\left[(\vec{S}\cdot\vec{v})\vec{v} - v^2\vec{S}\right], \tag{26}$$

where $\vec{v}$ is the speed of the satellite of mass m_s and $\vec{S}$ is the spin vector of the Earth. This is a spin-spin effect. Notice that this term does not have the dipolar nature of the usual FD effect. This term differs from the de Sitter effect which depends on the angular momentum of the bodies. Here the FD effect is proportional to the spin of the bodies.

Surprisingly and contrary to GR, the de Sitter effect coming from the scalar field follows from both the curvature in the Jordan frame h^J_{00} and the gravitomagnetic field $\vec{A}_J$. The FD effect itself follows from the curvature h^J_{00} sourced by the spin of the rotating bodies in the Klein-Gordon equation of the scalar field. However, we can still separate the de Sitter and FD contributions from the fact that the former depends on the angular momentum of the system and the latter on the spins.

C. Spin-orbit precession

In the following, we will compare the corrections to the spin-orbit and spin-spin precessions using diverse projections of the time-averaged precession vectors over a period. Defining by $\langle\cdot\rangle$ this averaging procedure, we obtain

$$\langle\Delta\Omega^i\rangle = \beta^2 G m_2^2\epsilon^{ijk}\left(-\frac{1}{m_1+m_2}L_3^{jk} + \frac{4G}{\Lambda^2}L_6^{jk}\right), \tag{27}$$

where we have defined the tensors

$$L_n^{ij} = \left\langle\frac{r^i v^j}{r^n}\right\rangle. \tag{28}$$

The angular momentum always points in the normal direction $\vec{n}$ to the orbital plane and we obtain

$$\langle\Delta\vec{\Omega}\rangle = \Delta\Omega\vec{n}, \tag{29}$$

where

$$\Delta\Omega = \beta^2 G m_2^2\left(-\frac{1}{m_1+m_2}L_3 + \frac{4G}{\Lambda^2}L_6\right). \tag{30}$$

We set the normal vector $\vec{n}$ along the z axis and use L_n for the time average of the magnitude of the angular momentum (i.e. $L^{ij} = \epsilon^{ijk}L_k$). We can choose the orbital plane to be at $z = 0$. As a result, the component of the angular momentum along the z direction is given by

$$L_n = \left\langle\frac{r^x v^y - r^y v^x}{r^n}\right\rangle. \tag{31}$$

The Keplerian solution reads

$$\frac{r}{a} = \frac{1-e^2}{1+e\cos\theta}, \qquad \dot{\theta} = n_b\frac{\sqrt{(1-e^2)}}{(r/a)^2},$$

where θ is the true anomaly. Using this, we can get the velocities as a function of θ:

$$\begin{aligned} v^x &= \dot{r}\cos\theta + r\dot{\theta}\sin\theta = \frac{n_b a}{\sqrt{1-e^2}}\sin\theta(2e\cos\theta+1),\\ v^y &= \dot{r}\sin\theta - r\dot{\theta}\cos\theta, = -\frac{n_b a}{\sqrt{1-e^2}}(e\cos 2\theta + \cos\theta). \end{aligned} \tag{32}$$

We obtain the value of L_n by the average over the unperturbed trajectories,

$$\langle\mathcal{A}\rangle = \frac{1}{2\pi}\int_0^{2\pi} d\theta\frac{(1-e^2)^{3/2}}{(1+ec)^2}\mathcal{A},$$

which gives

$$L_3 = \frac{n_b}{a}\frac{1}{1-e^2}, \qquad L_6 = \frac{n_b}{a^4}\frac{1+3e^2+\frac{3}{8}e^4}{(1-e^2)^4}.$$

In the case of circular orbits we have the explicit expression

$$L_n = \frac{v}{r^{n-1}} = \frac{n_b a}{r^{n-1/2}}. \tag{33}$$

The general solution for the spin-orbit precession contribution gives

$$\begin{aligned} \langle\Delta\Omega_{dS}\rangle = &-\frac{m_2^2}{(m_1+m_2)^{1/2}}\frac{G^{3/2}}{a^{5/2}(1-e^2)}\\ &\times\left[\beta^2 - \epsilon_\Lambda\left(1+3e^2+\frac{3}{8}e^4\right)\right], \end{aligned} \tag{34}$$

where ϵ_Λ quantifies the disformal strength, as in Eq. (4). The disformal strength is affected by the frequency of the orbital motion, where higher frequencies give larger disformal contributions. This follows from the higher derivative nature of the disformal interaction. In the corresponding astronomical units

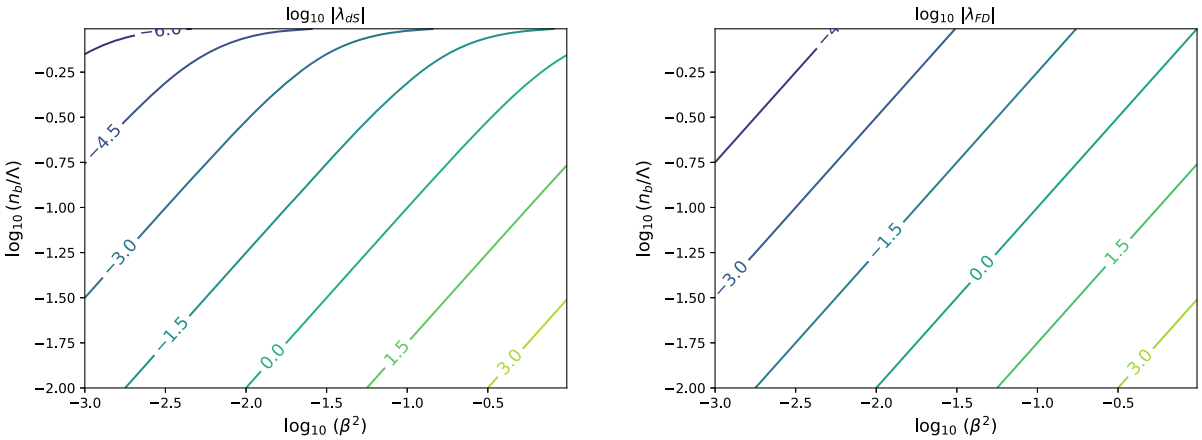

FIG. 2. Contour plots of the geodetic (left) and the frame-dragging effects (right). The contour shows the logarithm of the modification of the geodetic and the frame-dragging effects for different values of the conformal and disformal interactions, with $e \to 0$ and $m_1 \gg m_2$.

$$\Delta\Omega_{dS} = -\frac{T_\odot^{2/3} n_b^{5/3}}{1-e^2}\frac{m_2^2}{(m_1+m_2)^{4/3}} \times \left[\beta^2 - \epsilon_\Lambda\left(1+3e^2+\frac{3}{8}e^4\right)\right], \tag{35}$$

where $m \equiv m/M_\odot$ is the mass of the object in solar mass units and $T_\odot = GM_\odot/c^2$ is the scale of the period. In order to compare the contribution of the conformal and the disformal coupling to the GR one, we calculate the ratio between the de Sitter precession with the conformal and disformal interactions $\lambda_{dS} \coloneqq \Delta\Omega_{\rm dS}/\Omega_{\rm dS}^{\rm (GR)}$ to get

$$\lambda_{dS} = -\frac{2m_1}{3m_1+4m_2}\left[\beta^2 - \epsilon_\Lambda\left(1+3e^2+\frac{3}{8}e^4\right)\right]. \tag{36}$$

In the following section, we will analyze the complementary contribution coming from the FD effect. The left panel of Fig. 2 shows a contour plot of the geodetic effect. The contour shows the logarithm of the modification of the geodetic effect for different values of conformal and disformal interactions, with $e \to 0$ and $m_1 \gg m_2$. For the limit $m_2 \ll m_1$, the prefactor in the previous expression becomes $2/3$ and for the case $m_2 \sim m_1$ it is $2/7$. Finally, we notice that a nonvanishing eccentricity only enhances the contribution from the disformal coupling.

Let us comment on the PN corrections to this result compared to the disformal effect. In (36), the term in β^2 should be corrected at the next PN order by a term in $\beta^2 v^2$ where $v \ll 1$ is a typical velocity of the gyroscope. This term is negligible compared to the β^2 contribution but could compete with the disformal effect in ϵ_Λ. If $\beta^2 v^2 \ll \epsilon_\Lambda$, the disformal effect dominates over the conformal effect at the next PN order. On the other hand, when $\epsilon_\Lambda \lesssim \beta^2 v^2$, the disformal effect is negligible compared to the leading β^2 contribution. In all cases, we can trust formulas like (36) as the next PN order in $\beta^2 v^2$ does not play a significant role.

D. Frame-dragging precession

Similarly for the FD (or spin-spin) precession we introduce the tensor $T^{ij} = v^i v^j/r^6$ such that

$$\langle \Delta\Omega^i_{\rm FD}\rangle = -\frac{4\beta^2 G^2 m_s}{\Lambda^2}[S_j\langle T^{ij}\rangle - \langle T\rangle S^i], \tag{37}$$

where $T = T^i_i$ is the trace of the matrix T^{ij} which reads

$$\langle T^{ij}\rangle = \frac{GM(ec+1)^6}{a^7(1-e^2)^7}\begin{pmatrix} (s+es_2)^2 & -(2ce+1)(c+c_2e)s & 0 \\ -(2ce+1)(c+c_2e)s & (c+c_2e)^2 & 0 \\ 0 & 0 & 0 \end{pmatrix}, \tag{38}$$

where $\sin\theta = s$, $\cos\theta = c$, $\sin 2\theta = s_2$ and $\cos 2\theta = c_2$. The average gives

$$\langle T^{ij}\rangle = \frac{GM}{2a^7(1-e^2)^{11/2}}\begin{pmatrix} \frac{5e^6}{16}+\frac{41e^4}{8}+\frac{13e^2}{2}+1 & 0 & 0 \\ 0 & \frac{7e^6}{16}+\frac{61e^4}{8}+\frac{19e^2}{2}+1 & 0 \\ 0 & 0 & 0 \end{pmatrix}. \tag{39}$$

For circular orbits $e \equiv 0$ this reduces to

$$\langle T^{ij} \rangle = \frac{G(m_1 + m_s)}{2r^7}(\delta^{ij} - n^i n^j), \tag{40}$$

where $\vec{n}$ is perpendicular to the orbit. This implies that

$$\langle \Delta\vec{\Omega}_{\rm FD} \rangle = \frac{2\beta^2 G^3 m_s(m_1 + m_s)}{r^7 \Lambda^2}\left[(\vec{S}\cdot\vec{n})\vec{n} + \vec{S}\right]. \tag{41}$$

With the ansatz for the spin vector $\vec{S} = S\vec{z}$, we obtain the FD contribution from the disformal coupling

$$\langle \Delta\Omega^{\rm FD} \rangle = \frac{2\beta^2 G^3 (m_1 + m_s) m_s S}{a^7 \Lambda^2} \times \frac{1 + 8e^2 + \frac{51}{8}e^4 + \frac{3}{8}e^6}{(1-e^2)^{11/2}} \sin\psi. \tag{42}$$

This can be rewritten as

$$\langle \Delta\Omega_{\rm FD} \rangle = \epsilon_\Lambda \left(\frac{G m_s}{a c^2}\right) \frac{GS}{a^3} \frac{1 + 8e^2 + \frac{51}{8}e^4 + \frac{3}{8}e^6}{(1-e^2)^{5/2}} \sin\psi, \tag{43}$$

where ψ is the angle between the two spin vectors. Therefore, the modification for the frame-dragging precession rate $\lambda_{\rm FD} \coloneqq \Delta\Omega_{\rm FD}/\Omega_{\rm FD}^{\rm (GR)}$ gives

$$\lambda_{\rm FD} = \epsilon_\Lambda \Phi_s \frac{1 + 8e^2 + \frac{51}{8}e^4 + \frac{3}{8}e^6}{1 - e^2} \sin\psi \tag{44}$$

with the potential $\Phi_s = G m_s/(a c^2)$ of the satellite or the companion mass.

The functional dependence of the FD effect on the masses differs from the dS one. In particular, we see that they enter now via two dimensionless parameters, i.e. ϵ_Λ and Φ_s. The first one characterizes the ladder expansion and is only sensitive to the total mass of the system, whereas the second one is a characteristic of the satellite. In the dS case, the masses appear only as a dimensionless ratio $m_1/(3m_1 + 4m_2)$ which depends only on the mass ratio m_1/m_2. Note too the increased sensitivity on the conformal and disformal interactions for large eccentricities.

The right panel of Fig. 2 shows a contour plot of the FD effect. The contour shows the logarithm of the modification of the FD effect for different values of conformal and disformal interactions with $e \to 0$ and $m_1 \gg m_2$.

E. The prior and the likelihood

We perform a full Markov-chain Monte-Carlo (MCMC) analysis for different experiments. The parameter ϵ_Λ quantifies the contribution of the disformal interaction and depends on the orbital frequency of the body. Our prior is a flat prior with $\beta^2 \in [0, 1]$ and $\Lambda^{-1} \in [0, n_b^{-1}]$ where n_b is the orbital period of the system. We use an affine-invariant MCMC sampler for the minimization of our likelihoods via the implementation of the open-source package POLYCHORD [64]. Based on Ref. [65], the POLYCHORD estimates the evidence. One begins by drawing 400 live points uniformly from the prior. After some iterations, the point with the lowest likelihood is replaced by a new live point drawn uniformly from the prior with the constraint. The convergence is reached when the new evidence $Z_{\rm live}$ is some small fraction of the original one. The standard fraction of the POLYCHORD is $\epsilon < 0.01$.

The geodetic modification effect includes the conformal and the disformal couplings in two different parts, while the FD modification includes the conformal and the disformal contributions as a multiplicative factor. The FD experiments constrain the ratio β/Λ directly. In order to find a lower bound on Λ, we combine the FD results with the strong bound from the Cassini experiment taken as a Gaussian prior [8]. The bound reads

$$\beta^2 = (2.1 \pm 2.3) \times 10^{-5}, \tag{45}$$

where radio signals were sent from the Earth to the Cassini satellite and the Shapiro time delay was analyzed. In this case we take the conformal coupling β to be the same in the binary system environment and in the solar system. In the geodetic case the bound on β is independent of the Cassini bound. Similarly, in the analysis of Gravity Probe B, the experiment is embedded in the solar system so the bounds on β from this experiment can be compared directly to that of Cassini.

Finally, all our results depend on the ladder expansion of the disformal interaction. This requires that $\epsilon_L \ll 1$. We have checked that this is the case in our analyses. As $\epsilon_\Lambda \simeq v^2 n_b^2/\Lambda^2$ and as we impose a prior where $\Lambda^{-1} \in [0, n_b^{-1}]$, we see that $\epsilon_\Lambda \ll 1$ in all of the cases that we consider.

The likelihood for different experiments reads

$$-2\ln\mathcal{L}(\beta, \Lambda) = \sum_{i=1}^{N_{\rm PSR}} \left(\frac{\xi(\beta,\Lambda) - \xi_{ob}}{\delta\xi_{ob}}\right)^2, \tag{46}$$

where $\xi_{ob} \pm \delta\xi_{ob}$ is the observed precession vs the theoretical prediction $\xi(\beta, \Lambda)$ from the modified model with its dependence on the conformal and the disformal couplings.

III. SATELLITE EXPERIMENTS

In this section we discuss the bounds from current and future satellite experiments. Since the periods of these systems are in the same range, we expect to get similar bounds on the disformal coupling. As these experiments are all within the solar system, the bounds obtained here are on the couplings in this particular environment. In particular, when constraining the couplings using FD experimental

results, we will complement the measurements with the Cassini bound to deduce solar system constraints on the disformal coupling.

A. Gravity Probe B

Gravity Probe B (GPB) was a satellite-based experiment designed to test the geodetic and the FD effects. This was to be accomplished by measuring very precisely tiny changes in the direction of the spin of four gyroscopes contained in an Earth-orbiting satellite at 650 km. Reference [66] reports that analyses of the data from all four gyroscopes result in a geodetic drift rate of -6601.8 ± 18.3 mas/yr[3] and a FD drift rate of -37.2 ± 7.2 mas/yr, in good agreement with the general relativity predictions of -6606.1 ± 0.28 and -39.2 ± 0.19 mas/yr, respectively.

This provided a way to test different theories of gravity such as Yukawa-type potentials [67], Horava-Lifshitz gravity [68], light scalars or pseudoscalars coupled to leptons and affect the precessional [69]. and the first constraints on conformal and disformal interactions [28]. Since the orbital radius of the satellite is 7027.4 km, the orbital period is 0.0107 Hz $= 7 \times 10^{-19}$ eV. The posterior distribution of GPB is presented in Fig. 3. The complete MCMC yields a fit of

$$\beta^2 = (2.963 \pm 2.045) \times 10^{-3} \tag{47}$$

on the conformal coupling, giving $\Lambda > 3.92 \times 10^{-19}$ eV on the disformal coupling. The result is compatible with GR at the 2σ level. Taking the Cassini bound on the β parameter gives a bound of $\Lambda > 5.33 \times 10^{-21}$ eV on the disformal coupling. Notice that this is much higher than the Hubble rate now $H_0 \simeq 10^{-33}$ eV which would correspond to a suppression scale of the disformal coupling at the dark energy scale.[4]

B. LARES, LAGEOS and GRACE

The Laser Relativity Satellite (LARES)[5] was launched to measure the FD effect with an accuracy of about 10^{-2} [67,70–72]. The body of this satellite has a diameter of about 36.4 cm and weighs about 400 kg. The satellite was set on an orbit with an altitude of 1450 km, an inclination of 69.5 ± 1 degrees and eccentricity 9.54×10^{-4}. Tests of the FD precession consist of small secular precessions of the orbit of a test particle in motion around a central rotating mass. For example, this has been performed with the LAGEOS satellites [73] where the satellite acts as the particle moving around the earth. The orbital period of these systems is about 9×10^{-4} Hz $= 6 \times 10^{-19}$ eV. Since these experiments constrain the FD effect we complement them with the Cassini bound on the conformal coupling, and from these satellite experiments we get a range of $\Lambda > 10^{-20}$ eV on the disformal coupling. Figure 4 summarizes the different satellite experiments with the different constraints. Notice that all these experiments do not exclude the dark energy scale as a suppression scale for the disformal interaction.

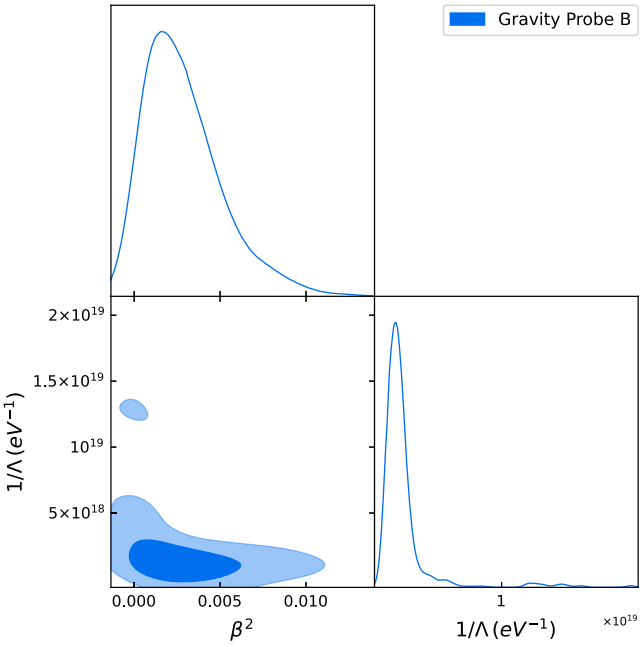

FIG. 3. Bounds on the conformal and the disformal couplings from the Gravity Probe B experiment which tests the geodetic and the FD effects and therefore gives a bound on the conformal coupling $(2.963 \pm 2.045) \times 10^{-3}$ and the disformal coupling $\Lambda > 3.92 \times 10^{-19}$ eV.

C. Gravity probe spin

In [74], it was suggested that future measurements of relativistic FD and geodetic precessions should use the intrinsic spin of the electron, hence called gravity probe spin (GPS). Such a measurement would be possible by using mm scale ferromagnetic gyroscopes in orbit around the Earth. Figure 5 shows the lower bound on the disformal coupling vs the future measurement error of the GPS experiment which is of the order of 10^{-18} eV.

[3]The term mas stands for milli-arc-second.

[4]The preferred value for disformal theories with an effect on the dynamics of the Universe is $\Lambda \simeq 10^{-33}$ eV. This follows from the presence of extra terms in the cosmological equations in ∂_t/Λ, i.e. time derivatives suppressed by the cutoff scale Λ. Typically, one expects dynamical effects from the scalar field when these terms are of order unity. Moreover, as the scalar field also evolves on time scales of the order of the age of the Universe H_0^{-1} at late times, i.e. when dark energy plays a role, this is only possible for a cutoff scale $\Lambda \simeq H_0$. As can be seen, this regime with a low cutoff scale is on the verge of the admissible energy range for a low energy effective field theory as higher order terms in the derivative expansion of the disformal term might be required.

[5]https://www.asi.it/scienze-della-terra/lares/.

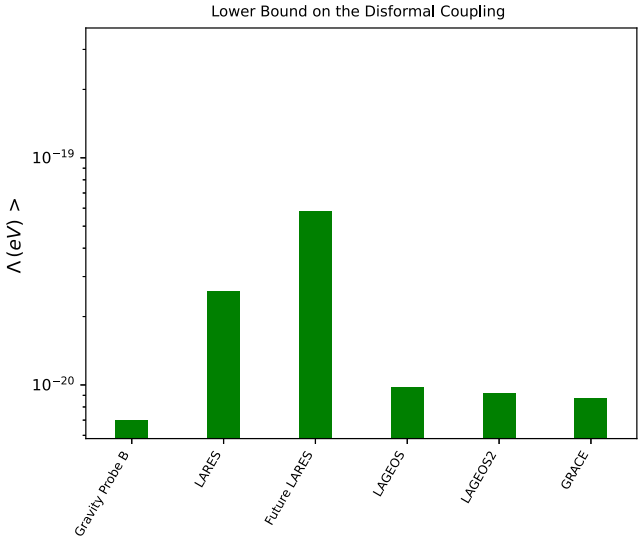

FIG. 4. The limit on the disformal coupling from the satellite experiments complemented with the Cassini bound on the conformal coupling. The range is compatible with $\Lambda > 10^{-19}$ eV.

IV. GINGER

GINGER (gyroscopes in general relativity) relies on the difference in time of flight of two counterpropagating waves in a closed path, i.e. the Sagnac effect [75–81]. The effect depends on the lack of reciprocity of the two directions and is related to the FD effect introduced by a rotating object. The difference in the time of flight is generated by the ring laser gyros which emit these counterpropagating waves. GINGER will measure the difference of time of flight with an accuracy down to $\sim 10^{-4}$ that will be used to test GR and other theories of gravity [82]. For the generic metric of a rotating gravitational object,

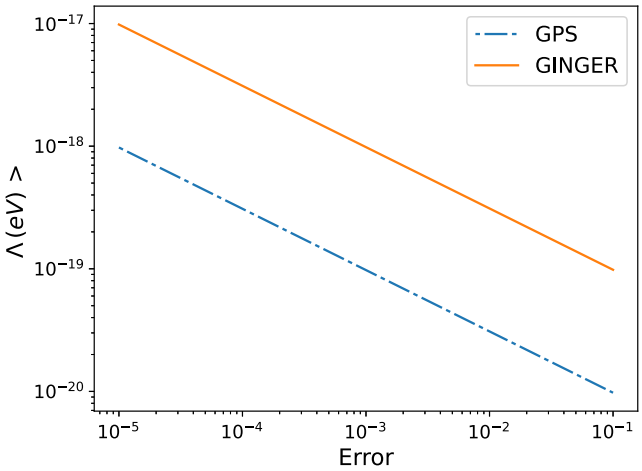

FIG. 5. The limit on the disformal coupling from the future GINGER and the gravity probe spin experiments in addition to the Cassini bound on the conformal coupling. The range is about $\Lambda > 10^{-17}$ eV for GINGER and $\Lambda > 10^{-18}$ eV for the gravity probe spin.

$$ds^2 = g_{00}dt^2 + 2g_{0i}dtdx^i + g_{ij}dx^i dx^j, \tag{48}$$

null geodesics are given by

$$dt = -\frac{g_{0i}}{g_{00}}dx^i - \frac{1}{g_{00}}((g_{0i}dx^i)^2 - g_{00}g_{ij}dx^i dx^j)^{1/2}. \tag{49}$$

Parametrizing the path that light follows in space in terms of a parameter l, and assuming a closed path of circumference P, i.e. $x^i(l) = x^i(l+P)$, we have the equations of the trajectory

$$\frac{dt}{dl} = -\frac{g_{0i}}{g_{00}}\frac{dx^i}{dl} - \frac{\epsilon}{g_{00}}\left(\left(g_{0i}\frac{dx^i}{dl}\right)^2 - g_{00}g_{ij}\frac{dx^i}{dl}\frac{dx^j}{dl}\right)^{1/2}, \tag{50}$$

where $g_{00} < 0$ and $dl = \epsilon|dl|$ with our choice of signature. We are interested in sending photons along the closed path in the two opposite directions with $(dl > 0)$ and $(dl < 0)$, respectively. The proper time delay between these two trajectories is given by

$$\Delta\tau = -2\sqrt{-g_{00}}\oint \frac{g_{0i}}{g_{00}}\frac{dx^i}{dl}dl. \tag{51}$$

The scalar field background influences this time delay as the metric considered here is the Jordan metric. Using the small field expansion, we get the leading order effect

$$\Delta\tau = 2\oint h^J_{0i}\frac{dx^i}{dl}dl = -\frac{4}{m_{\rm Pl}^2\Lambda^2}\oint \partial_0\varphi\partial_i\varphi\frac{dx^i}{dl}dl \tag{52}$$

which only involves the disformal coupling. As an example, a closed loop at the surface of a body considered as a test body in the field of a larger one, e.g. the Earth with its orbit around the Sun, will give rise to a time difference. Let us expand the field

$$\varphi(\bar{x} + x(l)) = \bar{\varphi} + x^i(l)\partial_i\bar{\varphi} + \cdots, \tag{53}$$

where $\bar{x}$ is the center of the loop while $\bar{\varphi}$ and its derivatives are their values at the center of the loop. The first nonvanishing contribution to the time delay is given by

$$\Delta\tau = \frac{4}{m_{\rm Pl}^2\Lambda^2}(\partial_0\partial_j\bar{\varphi}\partial_i\bar{\varphi} + \partial_0\bar{\varphi}\partial_i\partial_j\bar{\varphi})\oint x^j\frac{dx^i}{dl}dl. \tag{54}$$

Now for closed planar loops we have

$$\oint x^j\frac{dx^i}{dl}dl = A\epsilon^{jik}n_k, \tag{55}$$

where n_k is the unit vector orthogonal to the loop and A its surface area. With this we obtain the contribution of the disformal interaction to the time delay to be

$$\frac{\Delta\tau}{A} = \frac{4}{m_{\rm Pl}^2\Lambda^2}\epsilon^{ijk}\partial_0\partial_i\bar{\varphi}\partial_j\bar{\varphi}, \tag{56}$$

where A is the area encircled by the light beams. In the case of a loop at the surface of the Earth in the background of the Sun which is static in first approximation this becomes

$$\frac{\Delta\tau}{A} = \frac{128\pi G^2 m_\odot m_\oplus \beta^2}{\Lambda^2 r^3 d^3}\epsilon^{ijk}\left(v_i - 3\frac{(v^j r_j)}{r^2}r_i\right)d^j n^k, \quad (57)$$

where $\vec{v}$ is the velocity at the loop comprising the effects of the Earth's velocity in the heliocentric frame and the Earth's rotational velocity, $\vec{r}$ is the position of the center of the loop on Earth and $\vec{d}$ is the position of the Earth compared to the Sun. Using vectorial notation we have

$$\Delta\tau_{\rm dis} = \frac{128\pi G^2 m_\odot m_\oplus \beta^2}{\Lambda^2 r^3 d^2}\left((\vec{v} - 3v_r\vec{e}_r)\times\vec{d}\right)\cdot\vec{A}, \quad (58)$$

where $v_r = \vec{v}.\vec{e}_r$ and $\vec{e}_r = \frac{\vec{r}}{r}$. As expected, the time delay scales with the surface area of the loop and involves the projection of the angular momentum of the Earth around the Sun $\vec{d}\times\vec{v}$ along the normal to the loop $\vec{n}$. Finally, we denote by $\vec{A} = A\vec{n}$ the surface vector pointing in the normal direction to the loop. Based on [83] and performing the calculation in linear approximation for an instrument with its normal contained in the local meridian plane, the GR result is

$$\frac{\Delta\tau_{\rm GR}}{4\Omega_\oplus A} = \cos(\theta+\alpha) - 2\frac{GM}{R_\oplus c^2}\sin\theta\sin\alpha + \frac{GI_\oplus}{R_\oplus^3 c^2}(2\cos\theta\cos\alpha + \sin\theta\sin\alpha), \quad (59)$$

where α is the angle between the local radial direction and the normal to the plane of the instrument, measured in the meridian plane, θ is the colatitude of the laboratory, and $\Omega_\oplus$ is the rotation rate of the Earth as measured in the local reference frame.

In order to determine the contribution of $\Delta\tau_{\rm dis}$ we focus of the partial ratio, which gives

$$\frac{\Delta\tau_{\rm dis}}{\Delta\tau_{\rm GR}} \sim \frac{32\pi G^2 m_\odot m_\oplus \beta^2 v_E}{\Omega_\oplus \Lambda^2 R_\oplus^3 d^2}. \quad (60)$$

Since the future error of the GINGER experiment should be around 10^{-4} and taking the Earth velocity of order 30 km/sec, the lower limit on Λ should be around $> 3.1\times10^{-17}$ eV. In this case the dark energy scale would be strongly disfavored as a suppression scale for the disformal coupling. Figure 5 shows the lower bound on the disformal coupling vs the future measurement error of the GINGER experiment. This scaling assumption is compatible with the ladder expansion since the velocity we discuss here is much lower than the speed of light.

V. PULSARS

So far we have only considered satellites in the Earth's atmosphere. We change environment and consider precession effects further in the Milky Way where signals from pulsars have been observed. A pulsar is a highly magnetized rotating neutron star that emits radiation from its magnetic poles. This radiation can be observed only when a beam of emission is pointing towards the Earth (similar to the way a lighthouse can be seen only when the light points in the direction of an observer), and is responsible for the pulsed appearance of emissions. Binary pulsars are one of the best systems in astronomy in order to measure the post-Keplerian parameters (PKP) such as the orbital period decay $\dot{P}$ and the periastron advance $\dot{\omega}$. Reference [6] constrains light scalars with conformal and disformal interactions from the PKP. In the following we will assume that the conformal coupling in the pulsar's environment is the same as in the solar system. This will allow us to impose the Cassini bound on the conformal coupling when computing the posterior distribution of the conformal and disformal couplings.

The PKP which are accessible from the pulsar timings are the Einstein γ_E parameter accounting for the time delay due to the time dilation and the gravitational redshift of the pulsar signal in the solar system, the Shapiro time delays due to the crossing by the signal of the potential well of the solar system (this includes both the Shapiro delay shape s and the Shapiro delay range r, see [6] for their definition):

$$\gamma_E = e m_c \sqrt[3]{\frac{T_\odot^2}{n_b m}}(1+2\beta^2)^{2/3}\left(1+\frac{m_c}{m}\right),$$
$$s = \frac{x_p}{m_c}\sqrt[3]{\frac{n_b}{1+2\beta^2}\frac{m^2}{T_\odot}}, \qquad r = (1+2\beta^2)T_\odot m_c, \quad (61)$$

with the gravitational wave emission rate,

$$\dot{P} = -\frac{195\pi T_\odot^{5/3}}{5 n_b^{5/3}}\frac{m_p m_c}{m^{1/3}}\left[\left(1+\frac{\beta^2}{3}\right)f_1(e) + \frac{10}{9}\beta^2 f_2(e) - \epsilon_\Lambda\frac{20}{3}f_3(e)\right], \quad (62)$$

where

$$f_1(e) = \frac{1+\frac{73}{24}e^2+\frac{37}{96}e^4}{(1-e^2)^{7/2}}, \qquad f_2(e) = e^2\frac{1+\frac{1}{4}e^2}{(1-e^2)^{7/2}}$$
$$f_3(e) = e^2\frac{1+\frac{37}{4}e^2+\frac{59}{8}e^4+\frac{27}{64}e^6}{(1-e^2)^{13/2}}.$$

Finally we also include the periastron advance:

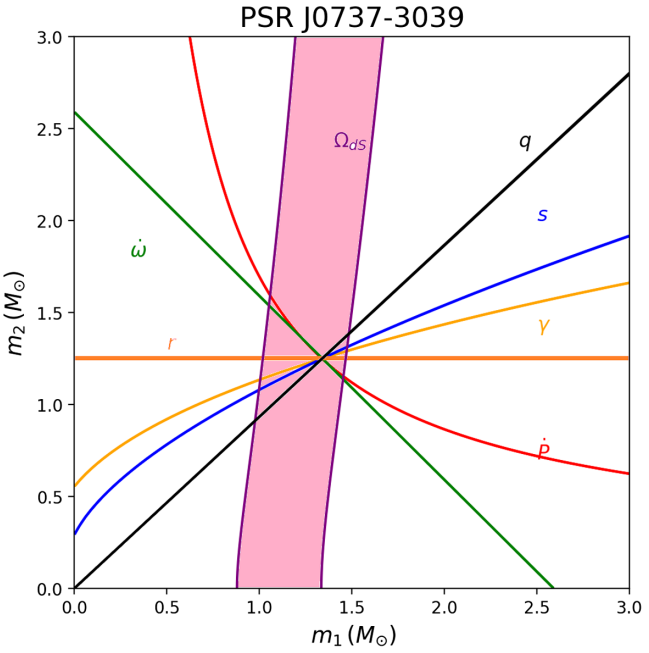

FIG. 6. The mass-mass diagram of the double pulsars PSR J0737-3039 A/B with the post-Keplerian parameters. The contour describes the post-Keplerian parameters and the width of each curve indicates the measurement uncertainty of the corresponding parameter.

$$\dot{\omega} = (mT_\odot)^{2/3} \frac{n_b^{5/3}}{1-e^2}\left[3 - 2\beta^2 + \frac{5\epsilon_\Lambda}{2\pi T_\odot \Lambda^2}\right]. \quad (63)$$

Here m_p is the pulsar mass, m_c is the companion mass, $m = m_p + m_c$ is the total mass of the system and x_p is the projected semimajor axis. These PKP provide a significant test of the conformal and disformal interactions leading to stringent constraints on the couplings of light scalars to matter.

In this paper we are interested in precession effects. It turns out that relativistic geodetic effects were detected and constrained using different binary pulsars. For instance, the pulsar PSR J1141-6545 gives results for the geodetic effect [84,85]. PSR J0737-3039 is a double pulsar [86] that gives a direct value for the geodetic precession [87,88]. We include the geodetic precession in the likelihood analysis that we perform in order to constrain the masses m_p and m_c together with the couplings β and Λ. The PKP involve the four unknown quantities m_p, m_c, β, Λ which should be extracted from the observables n_b, e, x_p, r, s, $\dot{P}_b$. This can be achieved from the likelihood

$$-2\ln\mathcal{L}(m_p, m_c, \beta, \Lambda) = \sum_{i=1}^{N_{\rm PSR}} \left(\frac{\xi(m_p, m_c, \beta, \Lambda) - \xi_{ob}}{\delta\xi_{ob}}\right)^2, \quad (64)$$

where ξ is one of the corresponding PKP taken from the list $\xi \in [\dot{\omega}, \dot{P}, \gamma_E, r, s, q, \Omega_{dS}]$ with the error $\delta\xi$. Here q is the ratio of the masses $q = m_p/m_c$. The priors we consider for the PKP are Gaussian priors as reported in the original papers. For the masses we put a uniform prior of $[0, 3]M_\odot$. Since the conformal interaction could be present without the disformal interaction, we test two different cases: only the conformal interaction and the conformal with the disformal interaction.

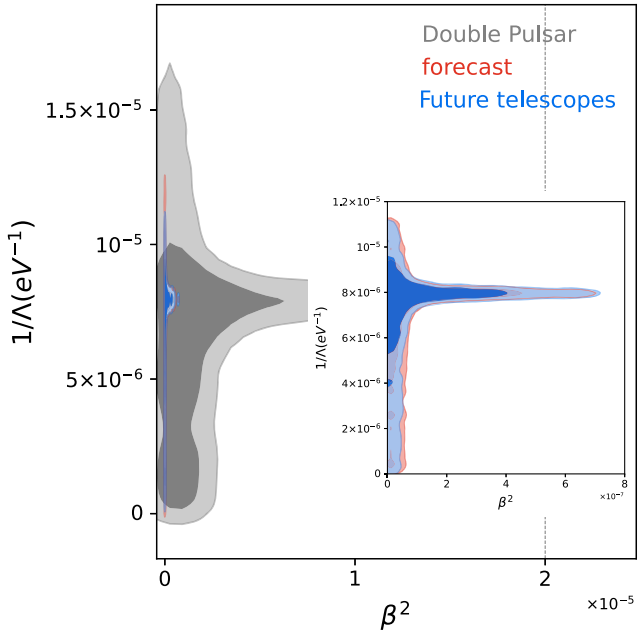

	β^2	$\Lambda\,(\mathrm{MeV}) >$
Current	$(1.94 \pm 0.72)\times 10^{-5}$	1.62
Forecast	$(1.16 \pm 1.84)\times 10^{-7}$	2.1
Future telescopes	$(0.99 \pm 1.53)\times 10^{-7}$	3.0

FIG. 7. The posterior probability distribution for the conformal and the disformal couplings (with 1σ and 2σ contours) after taking into account the measurements from PSR J0737-3039 A/B (gray). The forecast for future constraints on the conformal and the disformal interactions are given from PSR J0737-3039 A/B (red) and including future telescopes (blue). For future measurements, the covered area reduces and the upper bound on the conformal coupling and the lower bound on the disformal coupling changes.

Figure 7 shows the posterior probability distribution for the conformal and the disformal interactions from two different analyses. As the PKP depend on the masses of the pulsars and the companion star, the conformal and the disformal interactions, one has to use at least four PKP to extract constraints from data. The table and Fig. 7 shows the resulting constraints for the scalar interactions. We include in our analysis the de Sitter precession Ω_{dS}. One can see that the resulting bounds are strong and comparable to the Cassini bound (the gray line): $\beta^2 = (1.939 \pm 0.724) \times 10^{-5}$ and $\Lambda > 1.62$ MeV. This result is compatible with GR at the 2σ level.

Figure 6 shows the mass-mass diagram of the double pulsar. Any two lines give the contour of the corresponding

PKP (with a 1σ error) for different masses (the pulsar mass vs the companion star). In this case of coupled scalars, we include the best values of the conformal and the disformal interactions. Since the contours intersect at the same point in the mass-mass diagram, the model predicts the masses of the two pulsars and bounds the conformal and the disformal interactions up to the limit of the posterior values.

Reference [89] states that with additional years of timing measurements and new telescopes like the Square Kilometre Array (SKA) and others, the precision of these tests will increase and new effects like the FD precession of the orbit will become measurable. In this way, one could distinguish between the precession $\dot{\omega}$ and the FD precession $\dot{\omega}_{\rm FD}$ giving stronger constraints on the conformal and the disformal interactions.

Figure 7 shows the future constraint on the interactions using the forecast from Ref. [89]. Reference [89] uses simulations for future constraints with or without other telescopes to reduce current uncertainties. We use the future error that Ref. [89] estimates to be within reach in 2030 for different PKP. Future constraints should improve the bounds on the conformal and the disformal interactions, i.e. the conformal interaction upper bound will be at the 10^{-6} level and 10^{-7} when other telescopes are taken into account. The bound on the disformal interaction will be of the same order (∼MeV) but stronger when other telescopes are taken into account.

VI. S STARS IN THE GALACTIC CENTER

The center of the Milky Way hosts the closest supermassive black hole, Sgr A*. The stars orbiting Sgr A* are called S stars [58,90–99] with decades of monitoring of their locations and velocities. A large fraction of these stars have orbits with high eccentricities. Thus, they reach high velocities at the pericenter and can be used for constraining scalar interactions. There are a few studies that discuss the FD precession in the S-stars motion [100–104]. Reference [105] claims that the FD effect is overwhelmed by the systematic uncertainties in the Schwarzschild parameters due to the current errors in the stars' orbital parameters and the mass of Sgr A* itself. References [90,106] claim that detection of FD precession may be feasible after a few years' monitoring with an instrument like GRAVITY for orbits of some S stars. Especially, the S2 star orbits with a period of 16 years and it should be possible to constrain the angular momentum of the black hole by observing the star over 32 to 48 years. Reference [104] claims inconsistency between the current measurements of the Event Horizon Telescope predictions for the Sgr-A* spin and the bound from the S-stars orbits.

Using the known properties of the S stars (their masses and periods as in Ref. [107]) we forecast a bound on the disformal coupling, which depends on the errors of the future measurements of the quantities appearing in Eq. (44), i.e. the mass of the S stars, the eccentricity and the angle ψ. Figure 8 shows that we obtain a lower bound around $\Lambda > 10^{-5}$ eV after imposing the Cassini bound on the conformal coupling. We use the known masses of these S stars and the predicted accuracies of the future measurements. Other S stars around the galactic center have shorter periods than the S2 star, such as the S4711, S62, S4714 or S4716 [105,108] and will give stronger constraints on the disformal interaction. However, the masses of these stars are still unknown. This forecast only applies if the supermassive black hole at the center of the galaxy has a scalar charge. This could be the result of a violation of the no-hair theorem by the time dependence intrinsic to both the galactic and cosmological environments, see [109] for instance.

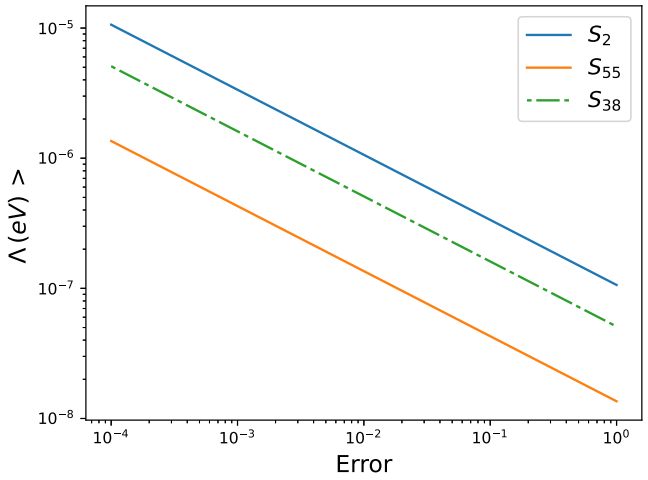

FIG. 8. Forecast of the lower bound on the disformal coupling from the frame dragging effect on some S stars in the galactic center combined with the Cassini bound on β.

VII. DISCUSSION AND SUMMARY

In this paper we investigated the consequences of a light scalar coupling to matter on the geodetic and the FD effects. Both conformal and disformal couplings of the scalar field to matter are considered and used to generate geodetic and FD effects. To first order in post-Newtonian expansion, the correction to the solution of the scalar field was obtained in [15]. This was extended in [6] to the post-Keplerian parameters with conformal and disformal interactions, enabling our current study.

Equations (36) and (44) show the relative modification to the geodetic and the FD precessions, respectively. If only the conformal interaction is present, then the geodetic effect is modified while the FD effect is affected only if both the conformal and the disformal couplings exist. The geodetic effect gives constraints on β directly and the FD effect gives constraint on β/Λ. For the experiments that measure the FD effect directly, we use the Cassini spacecraft bound on the conformal coupling as a prior, and deduce constraints on the disformal coupling.

The bounds on the coupling obtained from satellite experiments are strictly solar system constraints. This is why we can complement them with the Cassini bound. We find a bound on the disformal scale of order $\Lambda \gtrsim 10^{-18}$ eV which is much smaller than the one from pulsar timing $\Lambda \gtrsim 1$ MeV or even particle physics $\Lambda \gtrsim 650$ GeV. As the energy scales and the environments involved in pulsars and particle colliders are very different from the Earth's atmosphere, we simply notice that a strong variability with the environment is allowed for the disformal coupling.

The satellite-based experiments measure directly the FD effect while in the case of pulsars the effect is derived from the pulses sent to earth. Since the disformal interaction depends on the period, different systems with different periods will give different bounds. However, the satellite experiments have the advantage of measuring the FD effect directly.

The strongest bound on the conformal and disformal couplings from the geodetic effect is from the precession of binary pulsars and especially from the double pulsar [6]. The current observations of the double pulsar give a known bound on the geodetic precession value and in the near future one will be able to measure the FD precession directly [88]. Future measurements will help distinguish between the first and the second post-Newtonian contributions to the precessions and the FD contribution. With this separation the constraints on the disformal coupling should be more stringent with the increased precision on both $\dot{\omega}$ and $\dot{\omega}_{\rm FD}$. This will allow for a stronger test of light scalar couplings combining pulsar timing and precession effects.

ACKNOWLEDGMENTS

We would like to thank to Scott Melville, Leong-Khim Wong and the anonymous referee for useful comments and discussions. A. C. D. thanks Chandrima Ganguly for discussions and collaboration at an early stage of this work. D. B. thanks Pasha Fadeev and Jenny Wagner for useful discussions. D. B. gratefully acknowledges the support of the Blavatnik and the Rothschild fellowships. D. B. acknowledges a Postdoctoral Research Associateship at the Queens' College, University of Cambridge. D. B. received partial support from European COST actions CA15117 and CA18108 and the research Grant No. KP-06-N58/5.

APPENDIX: AVERAGES

We have defined the tensors $L_n^{ij} = \langle r^i v^j / r^n \rangle$ and the other cumulants that were not used in this paper, given by

$$
\begin{aligned}
L_0 &= \sqrt{a(1-e^2)G(m_1+m_2)}, \\
L_1 &= \sqrt{\frac{G(m_1+m_2)}{a}}\sqrt{1-e^2}, \\
L_2 &= \frac{1}{a}\sqrt{\frac{G(m_1+m_2)}{a}}, \\
L_4 &= \frac{1}{a^3}\sqrt{\frac{G(m_1+m_2)}{a}}\frac{1+e^2/2}{(1-e^2)^2} \\
L_5 &= \frac{1}{a^4}\sqrt{\frac{G(m_1+m_2)}{a}}\frac{1+3/2e^2}{2(1-e^2)^3}.
\end{aligned}
\tag{A1}
$$

[1] S. Perlmutter *et al.* (Supernova Cosmology Project Collaboration), Astrophys. J. **517**, 565 (1999).
[2] S. Weinberg, Rev. Mod. Phys. **61**, 1 (1989).
[3] P. J. E. Peebles and B. Ratra, Rev. Mod. Phys. **75**, 559 (2003).
[4] T. Baker *et al.*, Rev. Mod. Phys. **93**, 015003 (2021).
[5] A. Bassi, L. Cacciapuoti, S. Capozziello, S. Dell'Agnello, E. Diamanti, D. Giulini, L. Iess, P. Jetzer, S. K. Joshi, A. Landragin, C. L. Poncin-Lafitte, E. Rasel, A. Roura, C. Salomon, and H. Ulbricht, npj Microgravity **8**, 49 (2022).
[6] D. Benisty, P. Brax, and A.-C. Davis, Phys. Rev. D **107**, 064049 (2023).
[7] J. D. Bekenstein, Phys. Rev. D **48**, 3641 (1993).
[8] B. Bertotti, L. Iess, and P. Tortora, Nature (London) **425**, 374 (2003).
[9] J. Khoury and A. Weltman, Phys. Rev. Lett. **93**, 171104 (2004).
[10] P. Brax, C. van de Bruck, A.-C. Davis, J. Khoury, and A. Weltman, Phys. Rev. D **70**, 123518 (2004).
[11] K. Hinterbichler and J. Khoury, Phys. Rev. Lett. **104**, 231301 (2010).
[12] A. I. Vainshtein, Phys. Lett. **39B**, 393 (1972).
[13] T. Damour and A. M. Polyakov, Nucl. Phys. **B423**, 532 (1994).
[14] P. Brax, C. van de Bruck, A.-C. Davis, and D. Shaw, Phys. Rev. D **82**, 063519 (2010).
[15] P. Brax and A.-C. Davis, Phys. Rev. D **98**, 063531 (2018).
[16] P. Brax, C. Burrage, and C. Englert, Phys. Rev. D **92**, 044036 (2015).
[17] T. S. Koivisto, arXiv:0811.1957.
[18] M. Zumalacarregui, T. S. Koivisto, D. F. Mota, and P. Ruiz-Lapuente, J. Cosmol. Astropart. Phys. 05 (2010) 038.
[19] T. S. Koivisto, D. F. Mota, and M. Zumalacarregui, Phys. Rev. Lett. **109**, 241102 (2012).

[20] C. van de Bruck, J. Morrice, and S. Vu, Phys. Rev. Lett. **111**, 161302 (2013).
[21] P. Brax, C. Burrage, A.-C. Davis, and G. Gubitosi, J. Cosmol. Astropart. Phys. 11 (2013) 001.
[22] J. Neveu, V. Ruhlmann-Kleider, P. Astier, M. Besançon, A. Conley, J. Guy, A. Möller, N. Palanque-Delabrouille, and E. Babichev, Astron. Astrophys. **569**, A90 (2014).
[23] J. Sakstein, J. Cosmol. Astropart. Phys. 12 (2014) 012.
[24] J. Sakstein, Phys. Rev. D **91**, 024036 (2015).
[25] H. Desmond, B. Jain, and J. Sakstein, Phys. Rev. D **100**, 043537 (2019); **101**, 069904(E) (2020); **101**, 129901(E) (2020).
[26] S. Vagnozzi, L. Visinelli, P. Brax, A.-C. Davis, and J. Sakstein, Phys. Rev. D **104**, 063023 (2021).
[27] P. Brax, C. Burrage, and A.-C. Davis, J. Cosmol. Astropart. Phys. 09 (2011) 020.
[28] P. Brax, A.-C. Davis, S. Melville, and L. K. Wong, J. Cosmol. Astropart. Phys. 03 (2021) 001.
[29] C. van de Bruck and J. Morrice, J. Cosmol. Astropart. Phys. 04 (2015) 036.
[30] L. Hui, J. P. Ostriker, S. Tremaine, and E. Witten, Phys. Rev. D **95**, 043541 (2017).
[31] P. Brax, S. Fichet, and G. Pignol, Phys. Rev. D **97**, 115034 (2018).
[32] S. Trojanowski, P. Brax, and C. van de Bruck, Phys. Rev. D **102**, 023035 (2020).
[33] P. Brax, K. Kaneta, Y. Mambrini, and M. Pierre, Phys. Rev. D **103**, 015028 (2021).
[34] A. Maheshwari, E. Nissimov, and I. Todorov, Lett. Math. Phys. **5**, 359 (1981).
[35] T. Damour and J. H. Taylor, Phys. Rev. D **45**, 1840 (1992).
[36] A. Buonanno and T. Damour, Phys. Rev. D **59**, 084006 (1999).
[37] T. Damour and G. Schaefer, Nuovo Cimento Soc. Ital. Fis. **101B**, 127 (1988).
[38] T. Damour, P. Jaranowski, and G. Schaefer, Phys. Rev. D **62**, 044024 (2000).
[39] D. Benisty, Phys. Rev. D **106**, 043001 (2022).
[40] D. Benisty, N. W. Evans, and A.-C. Davis, Mon. Not. R. Astron. Soc. **518**, L51 (2022).
[41] D. Benisty, E. Vasiliev, N. W. Evans, A.-C. Davis, O. V. Hartl, and L. E. Strigari, Astrophys. J. Lett. **928**, L5 (2022).
[42] P. Brax, C. Burrage, and A.-C. Davis, J. Cosmol. Astropart. Phys. 10 (2012) 016.
[43] P. Brax, A.-C. Davis, and J. Sakstein, Classical Quantum Gravity **31**, 225001 (2014).
[44] X. Zhang, T. Liu, and W. Zhao, Phys. Rev. D **95**, 104027 (2017).
[45] A.-C. Davis and S. Melville, J. Cosmol. Astropart. Phys. 09 (2020) 013.
[46] P. Brax, A.-C. Davis, and A. Kuntz, Phys. Rev. D **99**, 124034 (2019).
[47] T. Liu, X. Zhang, and W. Zhao, Phys. Lett. B **777**, 286 (2018).
[48] M. Shibata and D. Traykova, Phys. Rev. D **107**, 044068 (2023).
[49] W. de Sitter, Mon. Not. R. Astron. Soc. **77**, 155 (1916).
[50] M. Bagchi, Universe **4**, 36 (2018).
[51] L. I. Schiff, Phys. Rev. Lett. **4**, 215 (1960).
[52] B. M. Barker and R. F. O'Connell, Phys. Rev. D **12**, 329 (1975).
[53] B. M. Barker and R. F. O'Connell, Astrophys. J. Lett. **199**, L25 (1975).
[54] B. M. Barker and R. F. Oconnell, Gen. Relativ. Gravit. **11**, 149 (1979).
[55] B. Mashhoon, F. W. Hehl, and D. S. Theiss, Gen. Relativ. Gravit. **16**, 711 (1984).
[56] H. Pfister, Gen. Relativ. Gravit. **39**, 1735 (2007).
[57] N. Yunes and X. Siemens, Living Rev. Relativity **16**, 9 (2013).
[58] D. Benisty and A.-C. Davis, Phys. Rev. D **105**, 024052 (2022).
[59] A.-C. Davis and S. Melville, J. Cosmol. Astropart. Phys. 11 (2021) 012.
[60] P. Brax, A.-C. Davis, S. Melville, and L. K. Wong, J. Cosmol. Astropart. Phys. 10 (2021) 075.
[61] M. H. L. Pryce, Proc. R. Soc. A **195**, 62 (1948).
[62] A. J. Hanson and T. Regge, Ann. Phys. (N.Y.) **87**, 498 (1974).
[63] C. Chicone, B. Mashhoon, and B. Punsly, Phys. Lett. A **343**, 1 (2005).
[64] W. J. Handley, M. P. Hobson, and A. N. Lasenby, Mon. Not. R. Astron. Soc. **450**, L61 (2015).
[65] J. Skilling, Bayesian Anal. **1**, 833 (2006).
[66] C. W. F. Everitt *et al.*, Phys. Rev. Lett. **106**, 221101 (2011).
[67] S. Capozziello, G. Lambiase, M. Sakellariadou, and A. Stabile, Phys. Rev. D **91**, 044012 (2015).
[68] N. Radicella, G. Lambiase, L. Parisi, and G. Vilasi, J. Cosmol. Astropart. Phys. 12 (2014) 014.
[69] T. K. Poddar, Eur. Phys. J. C **82**, 982 (2022).
[70] I. Ciufolini, E. Pavlis, F. Chieppa, E. Fernandes-Vieira, and J. Perez-Mercader, Science **279**, 2100 (1998).
[71] I. Ciufolini, A. Paolozzi, E. C. Pavlis, J. C. Ries, R. Koenig, R. A. Matzner, G. Sindoni, and H. Neumayer, Space Sci. Rev. **148**, 71 (2009).
[72] D. M. Lucchesi, M. Visco, R. Peron, M. Bassan, G. Pucacco, C. Pardini, L. Anselmo, and C. Magnafico, arXiv:1910.01941.
[73] I. Ciufolini and E. C. Pavlis, Nature (London) **431**, 958 (2004).
[74] P. Fadeev, T. Wang, Y. B. Band, D. Budker, P. W. Graham, A. O. Sushkov, and D. F. J. Kimball, Phys. Rev. D **103**, 044056 (2021).
[75] M. L. Ruggiero, Galaxies **3**, 84 (2015).
[76] A. Tartaglia, A. Di Virgilio, J. Belfi, N. Beverini, and M. L. Ruggiero, Eur. Phys. J. Plus **132**, 73 (2017).
[77] A. D. V. Di Virgilio, J. Belfi, W.-T. Ni, N. Beverini, G. Carelli, E. Maccioni, and A. Porzio, Eur. Phys. J. Plus **132**, 157 (2017).
[78] A. D. V. Di Virgilio *et al.*, Phys. Rev. Res. **2**, 032069 (2020).
[79] F. Bosi *et al.*, J. Phys. Conf. Ser. **1468**, 012243 (2020).
[80] A. D. Di Virgilio *et al.*, Eur. Phys. J. C **81**, 400 (2021); **81**, 457(E) (2021).
[81] C. Altucci *et al.*, in *Proceedings of the 16th Marcel Grossmann Meeting on Recent Developments in Theoretical and Experimental General Relativity, Astrophysics and Relativistic Field Theories* (World Scientific, Singapore, 2023), https://www.worldscientific.com/doi/10.1142/9789811269776_0329.

[82] S. Capozziello *et al.*, Eur. Phys. J. Plus **136**, 394 (2021); **136**, 563(E) (2021).
[83] F. Bosi *et al.*, Phys. Rev. D **84**, 122002 (2011).
[84] R. N. Manchester *et al.*, Astrophys. J. **710**, 1694 (2010).
[85] V. Venkatraman Krishnan, M. Bailes, W. van Straten, E. F. Keane, M. Kramer, N. D. R. Bhat, C. Flynn, and S. Osłowski, Astrophys. J. Lett. **873**, L15 (2019).
[86] M. Kramer *et al.*, Phys. Rev. X **11**, 041050 (2021).
[87] R. P. Breton, V. M. Kaspi, M. Kramer, M. A. McLaughlin, M. Lyutikov, S. M. Ransom, I. H. Stairs, R. D. Ferdman, F. Camilo, and A. Possenti, Science **321**, 104 (2008).
[88] M. Kramer, in *Proceedings of the 12th Marcel Grossmann Meeting on General Relativity* (World Scientific, Singapore, 2010), pp. 241–260, https://www.worldscientific.com/doi/abs/10.1142/9789814374552_0012.
[89] M. S. Kehl, N. Wex, M. Kramer, and K. Liu, in *Proceedings of the 14th Marcel Grossmann Meeting on Recent Developments in Theoretical and Experimental General Relativity, Astrophysics, and Relativistic Field Theories* (World Scientific, Singapore, 2017), Vol. 2, pp. 1860–1865, https://www.worldscientific.com/doi/abs/10.1142/9789813226609_0195.
[90] M. Grould, F. H. Vincent, T. Paumard, and G. Perrin, Astron. Astrophys. **608**, A60 (2017).
[91] Q. Yu, F. Zhang, and Y. Lu, Astrophys. J. **827**, 114 (2016).
[92] A. Boehle, A. M. Ghez, R. Schödel, L. Meyer, S. Yelda, S. Albers, G. D. Martinez, E. E. Becklin, T. Do, J. R. Lu, K. Matthews, M. R. Morris, B. Sitarski, and G. Witzel, Astrophys. J. **830**, 17 (2016).
[93] R. Abuter *et al.* (GRAVITY Collaboration), Astron. Astrophys. **615**, L15 (2018).
[94] S. Gillessen, F. Eisenhauer, T. K. Fritz, H. Bartko, K. Dodds-Eden, O. Pfuhl, T. Ott, and R. Genzel, Astrophys. J. Lett. **707**, L114 (2009).
[95] T. Do *et al.*, Science **365**, 664 (2019).
[96] R. Abuter *et al.* (GRAVITY Collaboration), Astron. Astrophys. **636**, L5 (2020).
[97] A. Amorim *et al.* (GRAVITY Collaboration), Mon. Not. R. Astron. Soc. **489**, 4606 (2019).
[98] M. Parsa, A. Eckart, B. Shahzamanian, V. Karas, M. Zajaček, J. A. Zensus, and C. Straubmeier, Astrophys. J. **845**, 22 (2017).
[99] B. Ben-Salem and E. Hackmann, Mon. Not. R. Astron. Soc. **516**, 1768 (2022).
[100] R. Kannan and P. Saha, Astrophys. J. **690**, 1553 (2009).
[101] F. Zhang, Y. Lu, and Q. Yu, Astrophys. J. **809**, 127 (2015).
[102] L. Iorio and F. Zhang, Astrophys. J. **839**, 3 (2017).
[103] L. Iorio, Mon. Not. R. Astron. Soc. **472**, 2249 (2017).
[104] G. Fragione and A. Loeb, Astrophys. J. Lett. **932**, L17 (2022).
[105] L. Iorio, Astrophys. J. **904**, 186 (2020); **941**, 209(E) (2022).
[106] D. Merritt, T. Alexander, S. Mikkola, and C. M. Will, Phys. Rev. D **81**, 062002 (2010).
[107] S. Gillessen, P. M. Plewa, F. Eisenhauer, R. Sari, I. Waisberg, M. Habibi, O. Pfuhl, E. George, J. Dexter, S. von Fellenberg, T. Ott, and R. Genzel, Astrophys. J. **837**, 30 (2017).
[108] F. Peißker, A. Eckart, M. Zajaček, and S. Britzen, Astrophys. J. **933**, 49 (2022).
[109] L. K. Wong, A.-C. Davis, and R. Gregory, Phys. Rev. D **100**, 024010 (2019).